ELSEVIER

Contents lists available at ScienceDirect

Organic Electronics

journal homepage: www.elsevier.com/locate/orgel





Alcohol assistant surface passivated perovskites for efficient perovskite solar cells

Luyao Zheng ^{a,1}, Lening Shen ^{a,1}, Unal Cagatay Yilmazoglu ^a, Tao Zhu ^a, Dong Zhang ^b, Jie Zheng ^b, Xiong Gong ^{a,b,*}

ARTICLE INFO

Keywords:
Perovskite solar cells
PbI₂ surface passivation
Alcohol treatment
Power conversion efficiency

ABSTRACT

The surface passivation has been intensively applied for diminishing surface defects, restricting leakage current and suppressing surface charge recombination, aimed to boost device performance of perovskite solar cells (PSCs). In this work, we report the utilization of alcohol to treat the surface of methylammonium lead iodide (CH₃NH₃PbI₃, MAPbI₃) thin film for generating excess PbI₂ as a surface passivation layer. X-ray diffraction, grazing-incident wide-angle x-ray scattering, and morphological studies reveal that additional PbI2 is indeed formed at the surface of MAPbI3 thin films with alcohol treatment. Photoluminescence studies demonstrate that the non-radiative charge recombination is suppressed within the butanol-treated MAPbI₃ thin film. The optimal film morphology is obtained from the butanol-treated MAPbI₃ thin film. The enlarged recombination resistance. reduced trap density, and improved build-in potential are observed from the PSCs based on the butanol-treated MAPbI3 thin film compared to those based on either pristine MAPbI3 or the ethanol- or isopropanol-treated MAPbI₃ thin films, respectively, indicating the surface charge recombination is restricted and the interface defects are suppressed within the butanol-treated MAPbI₃ thin film. As a result, a power conversion efficiency (PCE) of 20.44% is observed from the PSCs based on the butanol-treated MAPbI₃ thin film in comparison with a PCE of 17.24% from the PSCs based on the pristine MAPbI₃ thin film. Our findings demonstrate that we have developed a facile way to approach efficient PSCs through PbI2 surface passivation of MAPbI3 thin films with alcohol treatment.

In the past years, hybrid inorganic-organic perovskites, for example, methylammonium ($CH_3NH_3^+$, MA^+) lead triiodide, $MAPbI_3$, have been intensively investigated for realizing efficient perovskite solar cells (PSCs) [1–3]. Efficient PSCs based on the large grain-size polycrystalline perovskites have been reported, but studies found that the intrinsically inevitable electronic and structural disorders, the ionic point defects, and the extended dislocations within perovskites were limiting factors restricting device-performance of PSCs [3–8]. To suppress interfacial defects, manipulate band alignment, and prevent moisture, various materials have been used as the surface passivation layer [9–14]. It was also found that lead iodide (PbI₂), originating from extra PbI₂ in the perovskite precursors, could passivate interfacial defects, resulting in boosted photocurrent [15–18]. However, it is hard to avoid PbI₂ within bulk perovskites while previously maintaining PbI₂ at the surface of

perovskite thin films by using an extra ratio of PbI_2 in the perovskite precursors [16].

On the other hand, various alcohols have been extensively used as the solvent for organic spacer cations to create two-dimensional perovskites for approaching stable and efficient PSCs due to their good solubility for organic spacer cations rather than PbI₂ [19–22]. Thus, in principle, alcohols could be used to treat MAPbI₃ thin film to generate excess PbI₂ at the surface of MAPbI₃ thin films. However, using alcohols to treat the surface of MAPbI₃ thin films was rarely reported [23].

In this work, we report the utilization of ethanol, isopropanol, and but anol to treat the surface of MAPbI $_3$ thin film for generating excess PbI $_2$ as the passivation layer. Both x-ray diffraction and the grazing incident wide-angle x-ray scattering studies indicate that alcohol treatment does not affect the crystal structure of MAPbI $_3$ thin films but could

a School of Polymer Science and Polymer Engineering, College of Engineering and Polymer Science, The University of Akron, Akron, OH, 44325, USA

b Department of Chemical, Biomolecular, and Corrosion Engineering, College of Engineering and Polymer Science, The University of Akron, Akron, OH, 44325, USA

^{*} Corresponding author. School of Polymer Science and Polymer Engineering, College of Engineering and Polymer Science, The University of Akron, Akron, OH, 44325, USA.

E-mail address: xgong@uakron.edu (X. Gong).

 $^{^{1}}$ These authors are contributed to this work equally.

generates excess PbI_2 tiny crystals on the surface of $MAPbI_3$ thin films. Moreover, the alcohol treated $MAPbI_3$ thin films possess different film morphologies due to their different solubility for MAI. Photoluminescence studies demonstrate that the non-radiative charge recombination is suppressed within the butanol treated $MAPbI_3$ thin film. Furthermore, compared to pristine $MAPbI_3$ -based PSCs, an enlarged recombination resistance, a reduced trap density, and an improved build-in potential are observed from the PSCs based on the butanol-treated $MAPbI_3$ thin film, indicating the surface charge recombination is restricted and the interface defects are suppressed within $MAPbI_3$ thin film. As a result, a PCE of 20.44% is observed from the PSCs based on the butanol treated $MAPbI_3$ thin film in comparison with a PCE of 17.24% from the PSCs based on the pristine $MAPbI_3$ thin film.

1. Results and discussion

Fig. 1 presents the x-ray diffraction (XRD) patterns of pristine MAPbI $_3$ thin film and the MAPbI $_3$ thin films treated with ethanol, isopropanol, and butanol, respectively. All MAPbI $_3$ thin films possess a typical tetragonal perovskite structure with strong peaks representing (110), (220), and (314) planes [1,2]. Compared to pristine MAPbI $_3$ thin film, no obviously shifted peaks observed from the MAPbI $_3$ thin films treated with various alcohols indicate that alcohol treatment has a negligible effect on the crystal structure of MAPbI $_3$ thin films.

The grazing incident wide-angle x-ray scattering (GIWAXS) is carried out to investigate the surface of MAPbI3 thin films. Noted that the incident angle applied for the GIWAXS measurement is 0.14°, which is smaller than the critical angle (0.16°) of Si for the beamline condition. With such a small angle, the scattering pattern could provide surface information of thin film rather than bulk [26]. As shown in Fig. 2a, pristine MAPbI₃ thin film exhibits a mixture of scattered secondary spots and rings, especially the oriented (110) plane ($q = 1.0 \text{ Å}^{-1}$) along the azimuthal angle $\chi=0^\circ$ and $\pm 45^\circ$, which is corresponding to MAPbI₃. Fig. 2b presents the GIWAXS profile of the ethanol treated MAPbI₃ thin film. Except for the (110) plane, additional scattered spots of the (101) plane (q = 1.8 Å^{-1}), which is corresponding to PbI₂, indicates the formation of PbI2 small crystals on the top of MAPbI3 thin film. In addition, the scattered spots with q from 1.5 to 1.9 Å^{-1} merge within χ of 40° – 70° , which is attributed to PbI₂ thin film [25], indicates extra PbI₂ is on the surface of MAPbI₃ as well. Moreover, the (001) plane ($q = 0.9 \text{ Å}^{-1}$), corresponding to PbI₂, is oriented in the same χ as the (110) plane (q = 1.0 Å^{-1}), corresponding to MAPbI₃, indicating that PbI₂ is originated

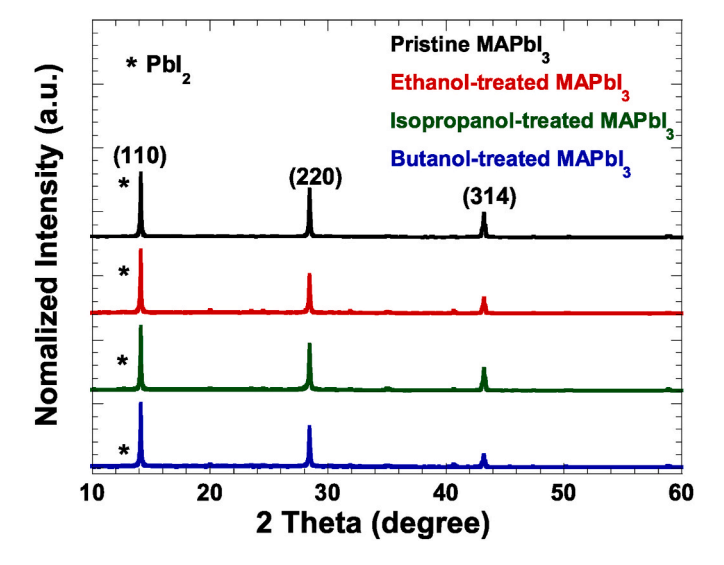


Fig. 1. The XRD patterns of pristine $MAPbI_3$ thin film and the $MAPbI_3$ thin films treated with ethanol, isopropanol and butanol, respectively.

from the decomposition of MAPbI $_3$ crystals during the ethanol treatment. As shown in Fig. 2c and d, the (001) plane ($q=0.9~\text{Å}^{-1}$) oriented in the $\chi\sim\pm~10^\circ$ indicates that either isopropanol or butanol treatment solely affects the surface rather than the bulk of MAPbI $_3$ thin films. Additionally, a ring-like scattered pattern of the (100) plane ($q=0.8~\text{Å}^{-1}$), corresponding to PbI $_2$, indicates that PbI $_2$ is randomly placed on the surface of MAPbI $_3$ thin films.

Top-view scanning electron microscopy (SEM) images of MAPbI₃ thin films are presented in Scheme 1. Pristine MAPbI₃ thin film possesses close-packed MAPbI3 crystals with a grain size of ~100 nm. With ethanol treatment, small crystals with a grain size less than ~10 nm, which is ascribed to PbI2, are found among MAPbI3 crystals. It was reported that the grain boundary is more favorable for structure disorders and point defects [4,7,8,17]. Thus, the formation of PbI₂ could first take place at grain boundaries as MAI is peeled off by alcohol treatment. Despite tiny PbI2 crystals being at grain boundaries, the "needle-like" PbI_2 crystals with a length of ~ 200 nm have appeared on the top of MAPbI₃ thin films, which are attributed to the excessive loss of MAI due to superior solubility of MAI in ethanol. Tiny PbI2 crystals are observed at grain boundaries of MAPbI₃ thin film treated with isopropanol. Less tiny PbI2 crystals observed from the MAPbI3 thin film treated with butanol compared to that with the isopropanol treated MAPbI₃ thin film are ascribed to poor solubility of MAI in butanol. On the other hands, the polarity of alcohols also plays a crucial role in the film morphology of the MAPbI₃ treated by various alcohols [23].

Atomic force microscopy (AFM) is further conducted to investigate the film morphologies of MAPbI₃ thin films. As shown in Scheme 2, pristine MAPbI3 thin film possesses a smooth surface with a root mean square of roughness (R_a) of 4.3 nm. A R_a is remarkably increased to 58.5 nm for the ethanol treated MAPbI₃ thin film, indicating a much rougher surface of the ethanol-treated MAPbI3 thin film. This observation is in good agreement with the SEM images (Scheme 1). Whereas, the isopropanol treated MAPbI $_3$ thin film exhibits a R_q of 4.6 nm, which indicates that PbI2 could be controlled by isopropanol treatment. Moreover, the butanol treated MAPbI₃ thin film exhibits a R_q of 3.5 nm, which indicates the butanol treated MAPbI₃ thin film possesses a smooth surface among all MAPbI3 thin films. Thus, the investigation of film morphologies of MAPbI3 thin films by SEM and AFM demonstrates that additional PbI2 could be formed on the surface of the MAPbI3 thin films treated with alcohol solvents and the butanol-treated MAPbI3 thin film possesses superior film morphology among all MAPbI₃ thin films, indicating that the PSCs based on the butanol-treated MAPbI3 thin film probably exhibit boosted J_{SC}.

The PSCs with an inverted structure of ITO/PTAA/MAPbI₃/PC₆₁BM/ Al, where ITO is indium doped tin oxide and acts as the anode, PTAA is poly[bis(4-phenyl) (2,4,6-trimethylphenyl)amine] and serves as the hole extraction layer (HEL), PC61BM is [6,6]-phenyl-C61-butyric acid methyl ester and serves as the electron extraction layer (EEL), and Al is aluminum and acts as the cathode, respectively, are fabricated and characterized. The current density-voltage (J-V) characteristics of PSCs are presented in Fig. 3a and the device-performance parameters are summarized in Table 1. The PSCs based on the pristine MAPbI₃ thin film exhibit a J_{SC} of 22.64 mA/cm², an open-circuit voltage (V_{OC}) of 1.04 V, a fill factor (FF) of 0.73, and a power conversion efficiency (PCE) of 17.24%, which well agrees with others' reports based on the similar device structure [27,28]. Whereas the PSCs based on the ethanol treated MAPbI₃ thin film exhibit a J_{SC} of 19.59 mA/cm², a V_{OC} of 1.02 V, a FF of 0.71, and a PCE of 14.23%. Such reduced device performance is ascribed to the poor morphology of the ethanol treated MAPbI3 thin film, even the formed PbI2 might function as the surface passivation layer. The PSCs based on the isopropanol treated MAPbI₃ thin film exhibit a J_{SC} of 24.84 mA/cm², a V_{OC} of 1.08 V, and a PCE of 19.11%. The optimal device performance is observed from the PSCs based on the butanol treated MAPbI₃ thin film exhibit a J_{SC} of 24.65 mA/cm² a 1.09 V, a FF of 0.76, and a PCE of 20.44%, which is \sim 20% enhancement compared with that based on the pristine MAPbI3 thin film.

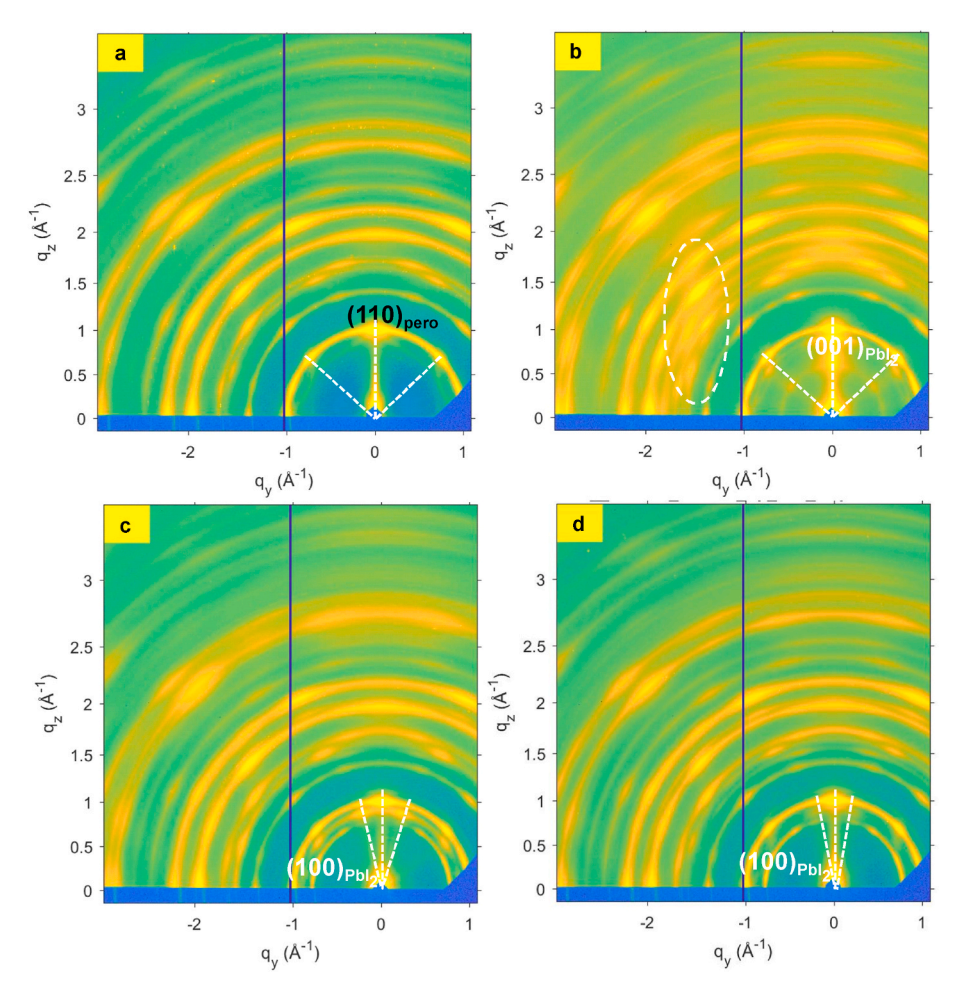


Fig. 2. The GIWAXS patterns of (a) pristine MAPbI₃ thin film, (b) the MAPbI₃ thin films treated with (b) ethanol, (c) isopropanol and (d) butanol, respectively.

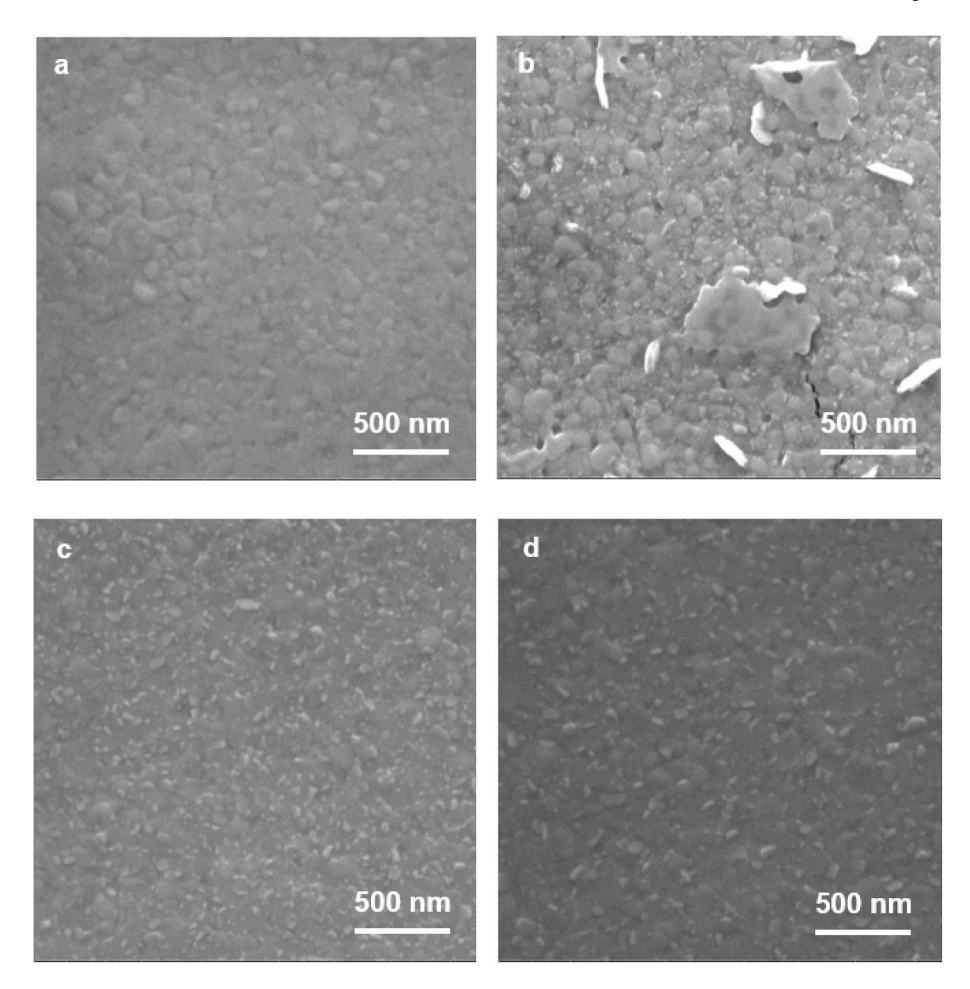
Fig. 3b displays the external quantum efficiency (EQE) spectra of PSCs. As compared with the PSCs based on the pristine MAPbI₃ thin film, reduced EQE values from 375 to 800 nm are observed from the PSCs based on the ethanol-treated MAPbI₃ thin film. Whereas, increased EQE values are found in both PSCs based on the isopropanol- and butanol-treated MAPbI₃ thin films. However, decreased EQE values are observed from the PSCs based on the isopropanol-treated MAPbI₃ thin film compared to that based on the butanol-treated MAPbI₃ thin film, which is probably ascribed to poor film morphology of the isopropanol-treated MAPbI₃ thin film compared to the butanol-treated MAPbI₃ thin film. The integrated photocurrent densities of 21.91 mA/cm², 18.88 mA/cm², 23.67 mA/cm², and 23.99 mA/cm² are calculated for the PSCs based on the pristine MAPbI₃ thin film, the ethanol-, or isopropanol-, or butanol-treated MAPbI₃ thin films. These values are in good agreement with those observed from the J-V characteristics (Fig. 3a).

In order to understand enhanced J_{SC} , absorption spectra of MAPbI $_3$ thin films are investigated. As indicated in Fig. 4a, all MAPbI $_3$ thin films possess the same optical cut-off values, indicating the optical bandgap of MAPbI $_3$ thin film is not affected by the alcohol treatment. Fig. 4b displays the photoluminescence (PL) spectra of MAPbI $_3$ thin films. Compared to pristine MAPbI $_3$ thin film, the ethanol-treated MAPbI $_3$ thin film possesses a significantly reduced PL intensity, indicating that the radiative charge recombination is reduced, which is probably originated from the formation of PbI $_2$ crystals on the surface of MAPbI $_3$ thin film. However, the enhanced PL intensities are observed in both isopropanoland butanol-treated MAPbI $_3$ thin films, indicating that the non-radiative charge recombination is suppressed. As a result, compared to the PSCs based on the pristine MAPbI $_3$ thin film, the PSCs based on the ethanol-treated MAPbI $_3$ thin film exhibit a poor PCE, but the PSCs based on

either the isopropanol- or but anol-treated $MAPbI_3$ thin films exhibit boosted PCEs values.

The shunt resistance (R_{sh}) and series resistance (R_s) estimated from the J-V characterizations of PSCs are summarized in Table 1. The PSCs based on the pristine MAPbI₃ thin film possesses a R_{sh} of 1.02 k Ω cm². Whereas, the PSCs based on the ethanol-treated MAPbI3 thin film possesses a R_{sh} of 0.91 k Ω cm². Such reduced R_{sh} indicates the leakage current is increased due to a rough surface of the ethanol-treated MAPbI₃ thin film (Scheme 2). As a result, a reduced J_{SC} is observed from the PSCs based on the ethanol-treated MAPbI₃ thin film. Such poor morphology of ethanol-treated MAPbI₃ thin film is responsible for both reduced V_{OC} and FF observed from the PSCs based on the ethanoltreated MAPbI₃ thin film. However, an enlarged R_{sh} of 6.33 k Ω cm² is observed from the PSCs based on the isopropanol-treated MAPbI₃ thin film. Such enlarged R_{sh} illustrates the leakage current at the interface is suppressed, indicating that additional PbI2 tiny crystals function as the passivation layer, thus resulting in enhanced J_{SC} . Similarly, an enlarged R_{sh} of 6.42 k Ω cm² accounted for the enhancement of J_{SC} in the PSCs based on the butanol treated MAPbI₃ thin film. In addition, the R_s is reduced to 4.97 Ω cm² for the PSCs based on the butanol treated MAPbI₃ thin film, from 8.66 Ω cm² for the PSCs based on the pristine MAPbI₃ thin film. Such reduced R_s demonstrate the improved charge carrier transport properties at the interface, implying that the charge carriers can efficiently pass through the interface before recombination for the PSCs based on the butanol-treated MAPbI₃ thin film. Thus, enhanced Voc and FF are observed from the PSCs based on the butanol-treated $MAPbI_3$ thin film.

Impedance spectroscopy (IS) is carried out to reveal charge carrier recombination in PSCs. Under illumination at a bias voltage close to $V_{\rm OC}$,



Scheme 1. The top-view SEM images of (a) pristine MAPbI₃ thin film and the MAPbI₃ thin films treated with (b) ethanol, (c) isopropanol, and (d) butanol, respectively.

the charge recombination resistance (R_{rec}) dominates in the equivalent circuit of PSCs [23]. Fig. 5a presents the Nyquist plot of PSCs. All PSCs exhibit one semicircle with a similar series resistance of 2 Ω at the high-frequency region. The R_{rec} is estimated by the radius of the semicircle. The PSCs based on the pristine MAPbI₃ thin film possess a R_{rec} of 86 Ω . A R_{rec} of 79 Ω is observed from the PSCs based on the ethanol-treated MAPbI₃ thin film, which indicates that a stronger charge carrier recombination takes place within PSCs. Whereas, dramatically increased R_{rec} of 368 Ω and 433 Ω are observed from the PSCs based on the isopropanol- and butanol-treated MAPbI₃ thin films, respectively. Over four times enlarged R_{rec} demonstrates a significantly suppressed interfacial charge recombination owning to PbI₂ surface passivation occurs within PSCs. The enlarged R_{rec} is consistent with the enlarged V_{OC} observed from the PSCs based on the isopropanol- and butanol-treated MAPbI₃ thin films.

The capacitance-voltage (C–V) measurement is further conducted to reveal the change in V_{OC} of PSCs. Fig. 5b presents the C^{-2} -V curves of PSCs. The build-in potential (V_{bi}) and the trap density (n_t) are ascribed based on the Mott-Schotty model [29]:

$$C^{-2} = \frac{2(V_{bi} - V)}{a\varepsilon\varepsilon_0 A^2 n_{\bullet}} \tag{1}$$

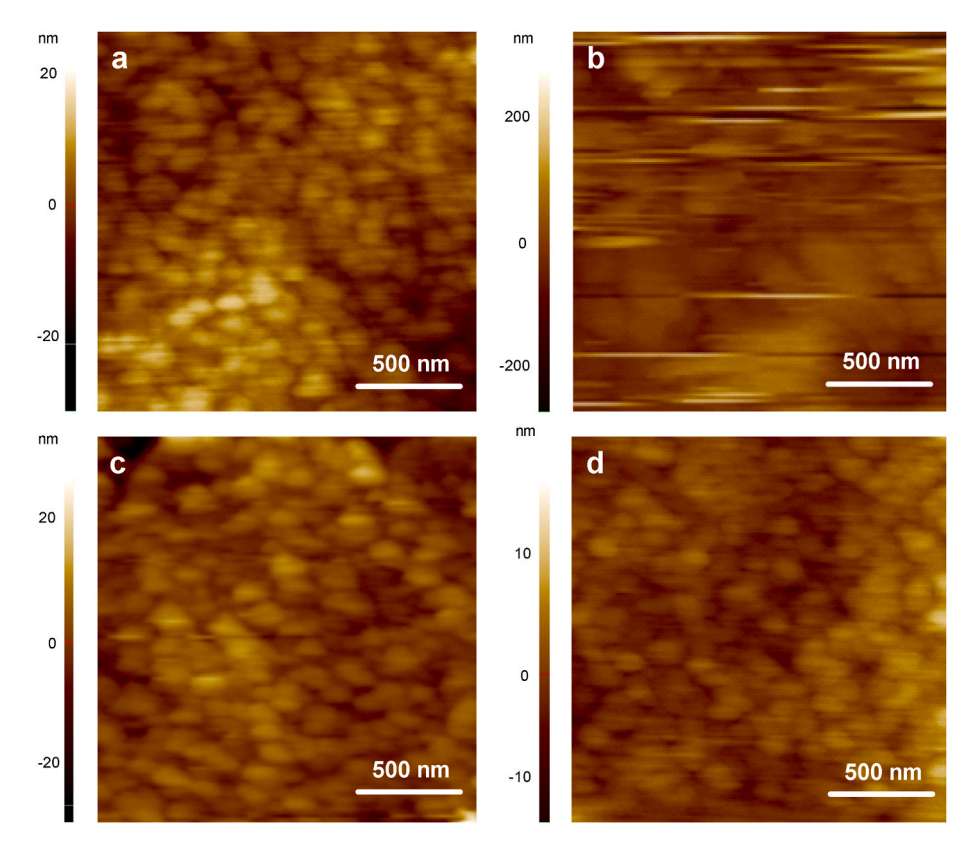
where V is applied bias, q is the elementary charge, ε is the dielectric constant of perovskites, ε_0 is the vacuum permittivity, and A is the active area, respectively. A V_{bi} of 1.10 V and a $n_{\rm t}$ of 4.1 \times 10¹⁵ cm⁻³ are observed from the PSCs based on the pristine MAPbI₃ thin film, whereas, the PSCs based on the ethanol-treated MAPbI₃ thin film possess a V_{bi} of 1.05 V and a $n_{\rm t}$ of 1.2 \times 10¹⁶ cm⁻³. A reduced V_{bi} and an increased $n_{\rm t}$

observed from the PSCs based on the ethanol-treated MAPbI $_3$ thin film are responsible for both reduced V_{OC} and J_{SC} . However, an enlarged V_{bi} of 1.14 V and a reduced n_t of 1.3 \times 10¹⁵ cm⁻³ are observed from the PSCs based on the isopropanol-treated MAPbI $_3$ thin film, resulting in enhanced V_{OC} and suppressed surface defects, thus a boosted J_{SC} . Furthermore, a V_{bi} of 1.16 V and a n_t of 1.1 \times 10¹⁵ cm⁻³ observed from the PSCs based on the butanol-treated MAPbI $_3$ thin film demonstrate that the surface of the butanol-treated MAPbI $_3$ thin film is well passivated through butanol treatment, indicating enlarged V_{OC} and boosted J_{SC} as well.

2. Methods

Materials: Lead iodide (PbI_2 , 99.9985%, metals basis) was purchased from Alfa Aesar. Methylammonium iodide (MAI, 99.9%) was purchased from GreatCell Solar. [6,6]-Phenyl- C_{61} -butyric acid methyl ester ($PC_{61}BM$) (99.5%) was purchased from Solenne BV. Poly[bis(4-phenyl) (2,4,6-trimethylphenyl)amine] (PTAA), methylamine (33 wt % in absolute ethanol), anhydrous acetonitrile (ACN, 99.8%), gamma-butyrolactone (GBL, 99%), toluene (99.8%), ethanol (99.5%), isopropanol (99.5%), butanol (99.8%) and chlorobenzene (CB, 99.8%) were purchased from Sigma-Aldrich. All chemicals were used as received without further purification.

MAPbI₃ single crystal: the growth of MAPbI₃ single crystal follows the inverse temperature crystallization method [24]. In brief, 1 mmol PbI₂, and 1 mmol MAI were dissolved in 1 mL GBL to make a clear solution. Then the solution was heated up to $110\,^{\circ}\mathrm{C}$ to let the single-crystal grow. The black crystals were collected and washed with isopropanol



Scheme 2. AFM images of (a) pristine MAPbI₃ thin film, and the MAPbI₃ thin films treated with (b) ethanol, (c) isopropanol and (d) butanol, respectively.

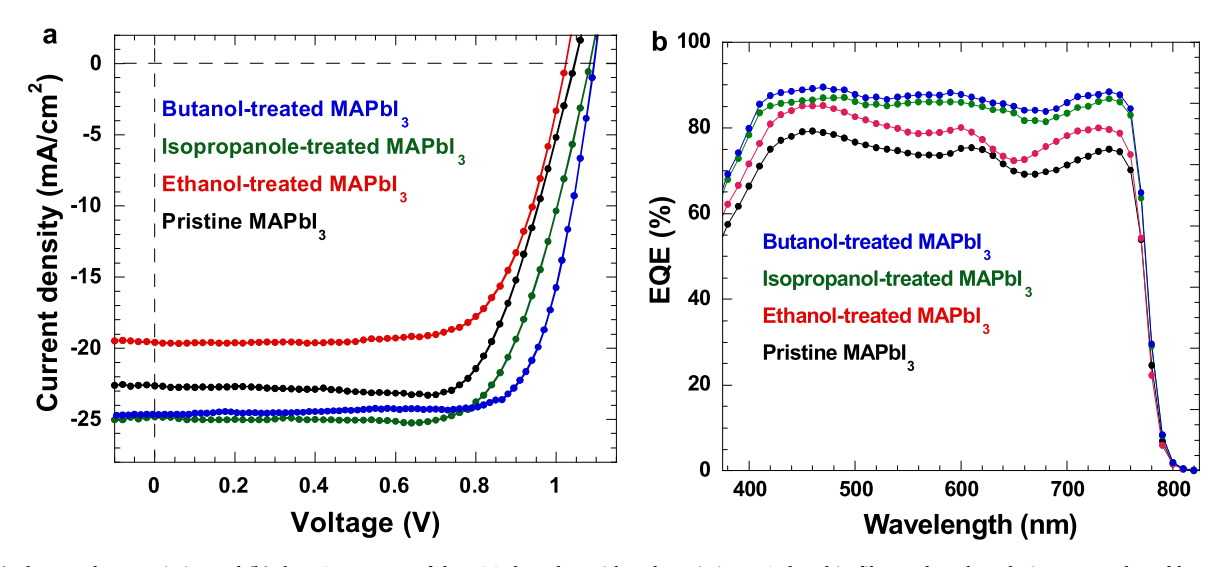


Fig. 3. (a) The J-V characteristics and (b) the EQE spectra of the PSCs based on either the pristine MAPbI $_3$ thin film or the ethanol-, isopropanol- and butanol-treated MAPbI $_3$ thin films, respectively.

three times and then dried out.

Perovskite precursor solution: the MAPbI₃ ACN solution was prepared following our previous reports [30]. The MAPbI₃ single crystal was placed in a small vial without the cap. Then the vial was sealed into a large bottle containing methylamine/ethanol solution. The methylamine gas diffused into the vial and exfoliated the MAPbI₃ single crystal into a viscous yellow solution, which was further diluted to 1 M with ACN.

Preparation of perovskite thin film: The $MAPbI_3$ thin film was deposited on the top of PTAA layer from the corresponding precursor solutions by spin coating at 6000 rpm for 30 s (s) and followed by

thermal annealing at 100 $^{\circ}\text{C}$ for 10 min (mins). For alcohol treatment, 80 μL alcohols were dripped on the top of MAPbI $_3$ thin film and kept for 5 s before spin coating at 6000 rpm for 30 s. Then, the alcohol-treated MAPbI $_3$ thin film was thermally annealed at 100 $^{\circ}\text{C}$ for 5 min.

Characterizations of perovskite thin film: X-ray diffraction (XRD) patterns of perovskite thin films were obtained from a Bruker AXS Dimension D8 X-ray system. The grazing-incident wide-angle X-ray scattering (GIWAXS) was performed on the dedicated high-resolution GIWAXS beamline (Sector 8-ID-E) in the Advanced Photon Source (APS), Argonne National Laboratory. X-ray photon energy was fixed at 10.92 keV. The incidence angle of 0.14° was used to check the scattering

Table 1 Device performance of the PSCs based on the $MAPbI_3$ treated with various alcohols.

Photoactive Layer	V _{oc} (V)	J _{SC} (mA/ cm ²)	FF (%)	PCE (%)	R_{sh} $(k\Omega$ $cm^2)$	R _s (Ω cm ²)
Pristine MAPbI ₃	$1.04 \\ \pm 0.01$	$\begin{array}{c} 22.64 \\ \pm \ 0.02 \end{array}$	73 ± 1	$17.24 \\ \pm 0.02$	1.02	8.66
Ethanol-treated MAPbI ₃	$\begin{array}{c} 1.02 \\ \pm \ 0.01 \end{array}$	$19.59 \\ \pm 0.02$	$\begin{array}{c} 71 \\ \pm \ 2 \end{array}$	$\begin{array}{c} 14.23 \\ \pm \ 0.02 \end{array}$	0.91	6.81
Isopropanol- treated	$\begin{array}{c} 1.08 \\ \pm \ 0.01 \end{array}$	$\begin{array}{c} 24.84 \\ \pm \ 0.02 \end{array}$	$\begin{array}{c} 71 \\ \pm 1 \end{array}$	$\begin{array}{c} 19.11 \\ \pm \ 0.02 \end{array}$	6.33	7.42
$MAPbI_3$ $Butanol-treated$ $MAPbI_3$	$\begin{array}{c} 1.09 \\ \pm \ 0.01 \end{array}$	$\begin{array}{c} 24.65 \\ \pm \ 0.02 \end{array}$	76 ± 1	$\begin{array}{c} 20.44 \\ \pm \ 0.02 \end{array}$	6.42	4.97

from the thin film surface. Perovskite thin films were coated on the silicon wafer, which was mounted on a rotating stage. The thin films and the stage were put in a vacuum to eliminate the moisture and oxygen influence on perovskite thin films during the measurement. Pilatus 1 M (Dectris Ltd.), a single-photon counter area detector, mounted at the position of either 212.4 mm downstream from the sample, was used to collect GIWAXS patterns. The GIWAXS data were collected by exposing thin films in X-ray for 10 s, and analyzed by using Matlab-based software

(GIXSGUI). Ultraviolet–visible (UV–vis) absorption spectra of thin films were measured using the HP 8453 spectrophotometer. The PL spectra were obtained on a Picoharp 300 instrument after pre-amplification by PAM 102. The top view scanning electron microscopy (SEM) images were obtained by using a field-emission scanning electron microscope (JEOL-7401). Atomic force microscopy (AFM) was conducted by Atomic Park System XE7 Atomic Force Microscopy.

PSCs Fabrication: The ITO glass was cleaned with detergent, deionized water, acetone, and isopropanol sequentially. Then, the ITO glasses were dried in an oven at 100 °C overnight. The pre-cleaned ITO substrates were then treated with UV-ozone for 40 min under an ambient atmosphere. Then, a \sim 8 nm thick PTAA was spin-casted on the top of ITO substrates from 2 mg/mL toluene solution and followed with thermal annealing at 100 °C for 10 min. The MAPbI₃ thin film was deposited on the top of the PTAA layer from the corresponding precursor solutions. After alcohol treatment, a 40 nm-thick PC₆₁BM layer was spin-cased on top of the perovskite layer from a 20 mg/mL chlorobenzene solution. Last, a 100 nm-thick aluminum (Al) was deposited through a shadow mask in the vacuum with the baseline of \sim 9 × 10⁻⁶ mbar atm. The device area was measured to be 0.043 cm².

PSCs Characterization: The density versus voltage (J-V) characteristics of PSCs were obtained by using a Keithley model 2400 source measure unit. A Newport Air Mass 1.5 Global (AM1.5G) full-spectrum solar simulator was applied as the light source. The light intensity was

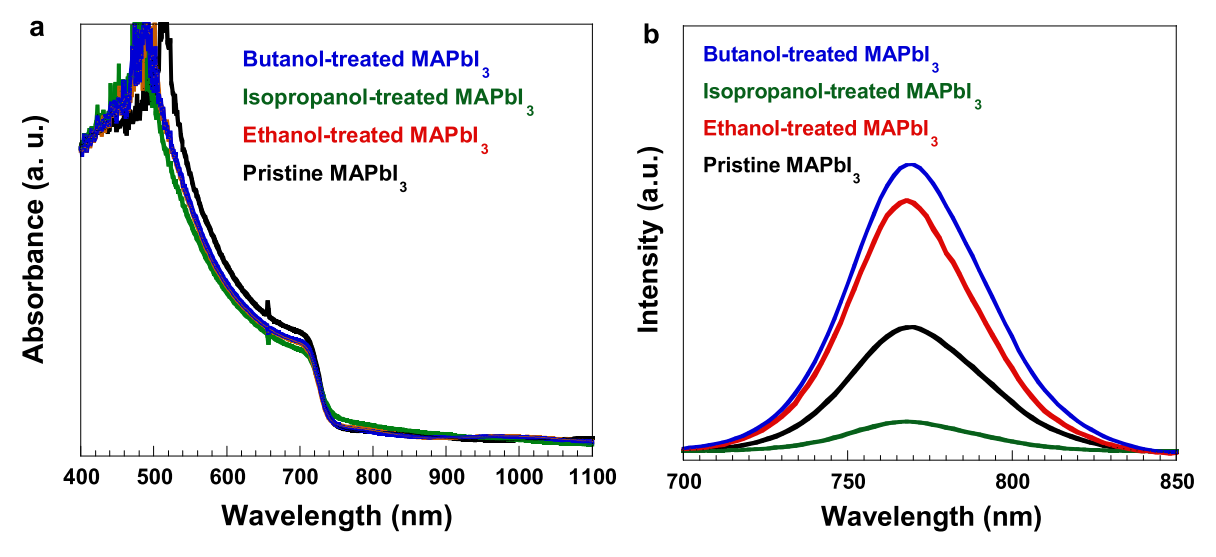


Fig. 4. (a) Absorption and (b) PL spectra of pristine MAPbI3 thin film and the ethanol-, isopropanol- and butanol-treated MAPbI3 thin films, respectively.

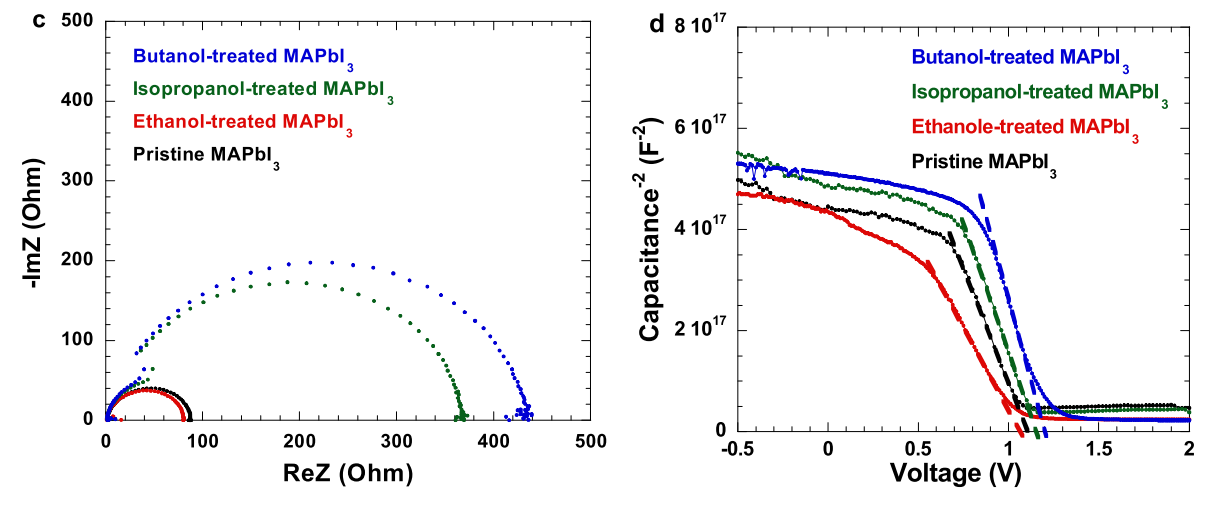


Fig. 5. (a) Impedance spectra of the PSCs based on either pristine MAPbI₃ thin film or the ethanol-, isopropanol- and butanol-treated MAPbI₃ thin films, respectively.

100 mW/cm², which was calibrated using a monosilicon detector (with a KG-5 visible color filter) from the National Renewable Energy Laboratory to reduce the spectral mismatch. The external quantum efficiency (EQE) measurement is obtained by using the solar cell quantum efficiency measurement system (QEX10) from PV measurements with a 300 W steady-state xenon lamp as the source light. Impedance spectra were recorded by an HP 4194A impedance/gain-phase analyzer with an oscillating voltage of 10 mV from 0.5 Hz to 1 MHz. The C–V measurements were carried out on an HP 4194A impedance/gain-phase analyzer in dark conditions, with an oscillating voltage of 10 mV under 10 kHz.

3. Conclusion

In summary, we demonstrated an efficient surface passivation method in PSCs by alcohol treatment. GIWAXS, optical, and morphological studies revealed that additional PbI $_2$ can be formed at the surface of MAPbI $_3$ thin film. However, inferior morphology was found in ethanol-treated MAPbI $_3$ thin film with degraded device performance of corresponding PSCs. The optimal MAPbI $_3$ thin film was obtained by butanol treatment. The enlarged $R_{\rm rec}$, increased $V_{\rm bi}$, and reduced $n_{\rm t}$ were observed in butanol-treated MAPbI $_3$ thin film compared with that in pristine MAPbI $_3$ thin film, indicating the restricted surface recombination induced by butanol treatment. As a result, an over 20% PCE was achieved in PSCs by butanol-treated MAPbI $_3$ thin film in comparison with 17% PCE observed from the PSCs based on the pristine MAPbI $_3$ thin film. Our findings developed a facility way to passive the surface of MAPbI $_3$ thin film by alcohols for efficient PSCs.

Declaration of competing interest

The authors declare that they have no known competing financial interests or personal relationships that could have appeared to influence the work reported in this paper.

Data availability

Data will be made available on request.

Acknowledgments

We thank the National Science Foundation (EECs 1903303) for financial support. We appreciate Dr. Qingteng Zhang, Dr. Joseph Strzalka, and Dr. Zhang Jiang at the Advanced Photon Source for the measurement and discussion of GIWAXS data.

References

- J.-P. Correa-Baena, M. Saliba, T. Buonassisi, M. Grätzel, A. Abate, W. Tress, A. Hagfeldt, Promises and challenges of perovskite solar cells, Science 358 (6364) (2017) 739–744.
- [2] J.-P. Correa-Baena, A. Abate, M. Saliba, W. Tress, T.J. Jacobsson, M. Grätzel, A. Hagfeldt, The rapid evolution of highly efficient perovskite solar cells, Energy Environ. Sci. 10 (3) (2017) 710–727.
- [3] M. Grätzel, The rise of highly efficient and stable perovskite solar cells, Acc. Chem. Res. 50 (3) (2017) 487–491.
- [4] J. Seo, J.H. Noh, S.I. Seok, Rational strategies for efficient perovskite solar cells, Acc. Chem. Res. 49 (3) (2016) 562–572.
- [5] L.M. Pazos-Outón, M. Szumilo, R. Lamboll, J.M. Richter, M. Crespo-Quesada, M. Abdi-Jalebi, H.J. Beeson, M. Vrućinić, M. Alsari, H.J. Snaith, Photon recycling in lead iodide perovskite solar cells, Science 351 (6280) (2016) 1430–1433.
- [6] L.M. Herz, Charge-carrier dynamics in organic-inorganic metal halide perovskites, Annu. Rev. Phys. Chem. 67 (2016) 65–89.

- [7] A. Walsh, D.O. Scanlon, S. Chen, X. Gong, S.H. Wei, Self-regulation mechanism for charged point defects in hybrid halide perovskites, Angew. Chem. Int. Ed. 54 (6) (2015) 1791–1794.
- [8] A. Buin, P. Pietsch, J. Xu, O. Voznyy, A.H. Ip, R. Comin, E.H. Sargent, Materials processing routes to trap-free halide perovskites, Nano Lett. 14 (11) (2014) 6281–6286.
- [9] H. Tan, A. Jain, O. Voznyy, X. Lan, F.P.G. De Arquer, J.Z. Fan, R. Quintero-Bermudez, M. Yuan, B. Zhang, Y. Zhao, Efficient and stable solution-processed planar perovskite solar cells via contact passivation, Science 355 (6326) (2017) 722–726.
- [10] H. Zhou, Q. Chen, G. Li, S. Luo, T.-b. Song, H.-S. Duan, Z. Hong, J. You, Y. Liu, Y. Yang, Interface engineering of highly efficient perovskite solar cells, Science 345 (6196) (2014) 542–546.
- [11] E.A. Alharbi, A.Y. Alyamani, D.J. Kubicki, A.R. Uhl, B.J. Walder, A.Q. Alanazi, J. Luo, A. Burgos-Caminal, A. Albadri, H. Albrithen, Atomic-level passivation mechanism of ammonium salts enabling highly efficient perovskite solar cells, Nat. Commun. 10 (1) (2019) 1–9.
- [12] S. Fu, X. Li, L. Wan, Y. Wu, W. Zhang, Y. Wang, Q. Bao, J. Fang, Efficient passivation with lead pyridine-2-carboxylic for high-performance and stable perovskite solar cells, Adv. Energy Mater. (2019).
- [13] S. Yang, S. Chen, E. Mosconi, Y. Fang, X. Xiao, C. Wang, Y. Zhou, Z. Yu, J. Zhao, Y. Gao, Stabilizing halide perovskite surfaces for solar cell operation with wide-bandgap lead oxysalts, Science 365 (6452) (2019) 473–478.
- [14] Y. Wang, T. Wu, J. Barbaud, W. Kong, D. Cui, H. Chen, X. Yang, L. Han, Stabilizing heterostructures of soft perovskite semiconductors, Science 365 (6454) (2019) 687–691
- [15] Y.C. Kim, N.J. Jeon, J.H. Noh, W.S. Yang, J. Seo, J.S. Yun, A. Ho-Baillie, S. Huang, M.A. Green, J. Seidel, Beneficial effects of PbI2 incorporated in organo-lead halide perovskite solar cells, Adv. Energy Mater. 6 (4) (2016), 1502104.
- [16] T.J. Jacobsson, J.-P. Correa-Baena, E. Halvani Anaraki, B. Philippe, S.D. Stranks, M.E. Bouduban, W. Tress, K. Schenk, J.I. Teuscher, J.-E. Moser, Unreacted PbI2 as a double-edged sword for enhancing the performance of perovskite solar cells, J. Am. Chem. Soc. 138 (32) (2016) 10331–10343.
- [17] T. Zhang, N. Guo, G. Li, X. Qian, Y. Zhao, A controllable fabrication of grain boundary PbI2 nanoplates passivated lead halide perovskites for high performance solar cells, Nano Energy 26 (2016) 50–56.
- [18] L. Wang, C. McCleese, A. Kovalsky, Y. Zhao, C. Burda, Femtosecond time-resolved transient absorption spectroscopy of CH3NH3Pbl3 perovskite films: evidence for passivation effect of Pbl2, J. Am. Chem. Soc. 136 (35) (2014) 12205–12208.
- [19] Z. Wang, Q. Lin, F.P. Chmiel, N. Sakai, L.M. Herz, H.J. Snaith, Efficient ambientair-stable solar cells with 2D–3D heterostructured butylammonium-caesiumformamidinium lead halide perovskites, Nat. Energy 2 (9) (2017), 17135.
- [20] D. Luo, W. Yang, Z. Wang, A. Sadhanala, Q. Hu, R. Su, R. Shivanna, G.F. Trindade, J.F. Watts, Z. Xu, Enhanced photovoltage for inverted planar heterojunction perovskite solar cells, Science 360 (6396) (2018) 1442–1446.
- [21] Y. Liu, S. Akin, L. Pan, R. Uchida, N. Arora, J.V. Milić, A. Hinderhofer, F. Schreiber, A.R. Uhl, S.M. Zakeeruddin, Ultrahydrophobic 3D/2D fluoroarene bilayer-based water-resistant perovskite solar cells with efficiencies exceeding 22, Sci. Adv. 5 (6) (2019) eaaw2543.
- [22] W.-Q. Wu, Z. Yang, P.N. Rudd, Y. Shao, X. Dai, H. Wei, J. Zhao, Y. Fang, Q. Wang, Y. Liu, Bilateral alkylamine for suppressing charge recombination and improving stability in blade-coated perovskite solar cells, Sci. Adv. 5 (3) (2019), eaav8925.
- [23] C. Liu, K. Wang, C. Yi, X. Shi, A.W. Smith, X. Gong, A.J. Heeger, Efficient perovskite hybrid photovoltaics via alcohol-vapor annealing treatment, Adv. Funct. Mater. 26 (1) (2016) 101–110.
- [24] M.I. Saidaminov, A.L. Abdelhady, B. Murali, E. Alarousu, V.M. Burlakov, W. Peng, I. Dursun, L. Wang, Y. He, G. Maculan, High-quality bulk hybrid perovskite single crystals within minutes by inverse temperature crystallization, Nat. Commun. 6 (2015) 7586.
- [25] K. Wang, L. Zheng, T. Zhu, X. Yao, C. Yi, X. Zhang, Y. Cao, L. Liu, W. Hu, X. Gong, Efficient perovskite solar cells by hybrid perovskites incorporated with heterovalent neodymium cations, Nano Energy 61 (2019) 352–360.
- [26] J.L. Baker, L.H. Jimison, S. Mannsfeld, S. Volkman, S. Yin, V. Subramanian, A. Salleo, A.P. Alivisatos, M.F. Toney, Quantification of thin film crystallographic orientation using X-ray diffraction with an area detector, Langmuir 26 (11) (2010) 9146–9151.
- [27] W. Xu, L. Zheng, T. Zhu, L. Liu, X. Gong, Bulk heterojunction perovskite solar cells incorporated with Zn2SnO4 nanoparticles as the electron acceptors, ACS Appl. Mater. Interfaces 11 (37) (2019) 34020–34029.
- [28] Q. Wang, C. Bi, J. Huang, Doped hole transport layer for efficiency enhancement in planar heterojunction organolead trihalide perovskite solar cells, Nano Energy 15 (2015) 275–280.
- [29] D.K. Schroder, Semiconductor Material and Device Characterization, John Wiley & Sons, 2015.
- [30] L.Y. Zheng, K. Wang, T. Zhu, Y.R. Yang, R. Chen, K. Gu, C.M. Liu, X. Gong, High-performance perovskite solar cells by one-step self-assembled perovskite-polymer thin films, ACS, Appl. Eng. Mater. (2020), https://doi.org/10.1021/acsaem.0c00823.